Paper No.
12

CORROSION 99

EFFECTS OF MULTIPHASE FLOW ON CORROSION INHIBITOR

Yue Chen
NSF I/UCRC, Corrosion in Multiphase Flow Systems Center
Dept. of Chemical Engineering
Ohio University
Athens, OH 45701

Huey J. Chen
Chevron Petroleum Technology Company
1300 Beach Boulevard
La Habra, CA 90631-6374

W. Paul Jepson
NSF I/UCRC, Corrosion in Multiphase Flow Systems Center
Dept. of Chemical Engineering
Ohio University
Athens, OH 45701

ABSTRACT

This paper investigates the inhibition performance of a typical imidazoline based inhibitor under multiphase flow. Electrochemical impedance spectroscopy (EIS) measurements were carried out in a 101.6 mm I.D., 15 m long acrylic flow loop using ASTM substitute saltwater and carbon dioxide gas. This flow loop system can generate slug flow, full pipe flow and other multiphase flow patterns. Effects of different flow conditions on inhibition performance of this typical inhibitor were examined. The system was maintained at a pressure of 0.136 MPa and a temperature of 40 °C. EIS measurements for this inhibitor in a Rotating Cylinder Electrode (RCE) system were also conducted. Different equivalent circuit models were used to fit the experiment data for both the RCE and flow loop systems. The high shear stress and turbulence due to the mixing vortex and the bubble impact in multiphase flow can enhance the corrosion or reduce the inhibition performance of inhibitors.

Keywords: Electrochemical impedance spectroscopy (EIS), corrosion inhibitor, corrosion inhibition, electrical equivalent circuit models, multiphase flow, flow loop

INTRODUCTION

Corrosion inhibitors play an important role in preventing internal corrosion in carbon steel pipelines that transport mixture of oil, water, natural gas and carbon dioxide gas. Imidazoline based corrosion inhibitors are well known to have a high inhibition activity to minimize carbon dioxide-induced oil field corrosion. The successful selection of inhibitors depends on a clear understanding of the operational conditions, fluid properties, solution pH and chemistry, and flow conditions. Fluid conditions include flow velocity and water cut. Inability to predict the flow patterns in multiphase pipelines could seriously affect the inhibitor selection, and thus reduce its effectiveness [1].

Multiphase flow can be classified into many different flow patterns as shown in Figure 1. At high production rates, the slug flow regime is prominent. The profile of a slug is shown in Figure 2[2]. Ahead of a slug, a concurrent slow moving liquid film flows with gas above it. The high gas velocity results in waves at the interface. These waves grow with increasing in liquid flow and bridge the pipe. The higher gas velocity accelerates these, forming a fast moving slug. A mixing zone is created in this process. This leads to a scouring mechanism on the pipe wall with the high rate of shear. As the liquid is scooped up into the slug, the leading edge of the slug jumps to the top of the pipe and entrains considerable amounts of gas. This results in a highly frothy turbulent region behind the slug front. The gas in the mixing zone is in the form of pulse of bubbles. These bubbles are trapped by the mixing vortex and shot to the bottom of the pipe where they can impact and collapse on the pipe walls. A slug flow is known to significantly enhance internal corrosion in oil/water/gas pipelines [3-4]. This is due to the high levels of shear and turbulence occurring in slug mixing zone [5-7].

Slug flow is characterized by Froude number Fr [10], which is defined as following formula:

$$Fr = \frac{Vt - V_f}{\sqrt{g * h_{eff}}} \qquad (1)$$

Where V_t = translational velocities of the slug front, m/s;
V_f = average velocity of the liquid film, m/s;
g = the acceleration due to gravity, m/s^2 ;
h_{eff} = the effective height of the liquid film, m.

The inhibition performance of corrosion inhibitors has been studied by various researchers. They [8-9] carried out their studies in RCE or small-scale flow loop using brine saturated with carbon dioxide. These test systems do not often represent the real flow conditions.

EIS measurements involve applying a small potential to the electrode surface. The current response to the applied potential can differ in phase and magnitude. Measurement of the difference in phase and amplitude permits analysis of the electrode process in relation to contributions from diffusion, charge transfer, double layer and inhibitor film. EIS offers some distinct advantages over conventional methods. EIS is a very useful tool for providing information on inhibitor film growth and for generating parameters, which are specific to a particular corrosion inhibitor system. Equivalent electrical circuit model provides a helpful way to interpret and quantify the EIS spectra if the physical models are understood.

This paper presents results for the study on inhibition performance of an imidazoline based corrosion inhibitor package formulated with imidazoline salt and quaternary amine under multiphase

flow conditions using EIS. The results for this inhibitor package in RCE system were compared with those under multiphase flow.

EXPERIMENTAL PROCEDURE

Multiphase Flow loop

Experiments were carried out in a 101.6 mm I.D., 15 m long acrylic flow loop. The schematic layout of the system is shown in Figure 3(a). It is similar to the one designed by Jepson[10]. A prepared ASTM substitute saltwater is placed in the 1.4 m^3 stainless steel tank A. The liquid from the tank is pumped into the 76 mm I.D. PVC pipe by 1.5 kW centrifugal pump. The flow rate of the liquid is controlled by a bypass line B and is measured by a calibrated orifice meter D. Liquid is passed into a 76 mm I.D. PVC pipe and then forced under gate E into the 101.6 mm I.D. plexiglass pipe where it formed a fast moving liquid film. The carbon-dioxide gas is introduced into the system at port F. The gas-liquid mixture passes through the plexiglass pipeline and enters the tank where the liquid is separated using a de-entrainer plate inside the tank. Liquid is recycled and gas is vented to the atmosphere through the exhausted at the top of the tank. The carbon dioxide gas is also used to pressurize the system. The pressure inside the tank is indicated by the gauge I, installed on the top of the tank. All the measurements are taken in the test section G located 8 m downstream from the gate. For slug flow, a hydraulic jump is generated and moved to the test section by controlling the gas flow at the inlet F. This is done using a needle valve in conjunction with a flow control system. The liquid inside the tank is heated by two 1.5 kW heater positioned at K. The EIS probe and coupons were inserted into the test section G shown in Figure 3(b), and are flush mounted with the pipe wall. The EIS probe consists of three electrodes. The working electrode is made of carbon steel. The counter and reference electrodes are made of stainless steel. The surface area of the electrode is 0.785 cm^2.

Tests were performed using saltwater and carbon dioxide gas. Once the de-oxygenation process is completed, the EIS probe is polished by 600-grid sandpaper , rinsed with acetone and distilled water and then inserted into the test section and EIS measurements are started. For slug flow experiments, the liquid flow rate is adjusted to a value required to given the desired Froude number and the liquid is forced through the gate. At this point a hydraulic jump is created. The hydraulic jump is stationary inside the test section with the control system on the gas line. Full pipe flow was studied for liquid velocity of 1.25 m/s and slug flow for Froude numbers 6 and 9. The system temperature and pressure are maintained constant at 40 °C and 0.136 MPa for all experiments. The concentration of the inhibitor was 25 ppm based on the total fluid.

Rotating Cylinder Electrode

The electrochemical cell is schematically shown in Figure 4(a). The working electrode is C-1018 mild steel with a total area of 3.02 cm^2. The counter electrodes are two graphite electrodes, and the reference electrode is a Saturated Calomel Electrode (SCE) connected to a salt bridge. The electrochemical cell containing 250 ml of saltwater was de-aerated with CO_2 for 1 hour to ensure CO_2 saturation of the brine.

A coupon as shown in Figure 4(b) was pre-polished with 600-grid sandpaper, rinsed with distilled water and acetone. The coupon was installed on the shaft and placed into the cell as the working electrode. The solution was stirred using a stirrer at 1000 rpm and CO_2 was continuously sparged into the system. Temperature was maintained at 40 °C. The concentrations of the inhibitor tested were 10 and 25 ppm.

All data were taken using the EIS electrochemical measurement system. EIS measurements were carried out at open circuit potentials with amplitude of 10 mV in the frequency range about 20 mHz to 5 kHz. For the RCE system, EIS measurements were conducted 2 hours after coupon immersion to establish the baseline data. The inhibitor of desired concentration (e.g. 25 ppm) was then injected into the cell after the pre-corrosion step. EIS measurements were conducted every hour during time of inhibition testing. For the flow loop tests, two kinds of experimental procedures were used. One was the same as REC system, which had the pre-corrosion step. EIS measurements were conducted 2 hours after coupon immersion to take the baseline data, followed by inhibitor addition. For inhibition testing in flow loop without pre-corrosion, the probe was placed in the inhibitor containing system directly. EIS measurements were conducted every hour during the inhibition testing for both experiments.

EQUIVALENT CIRCUIT MODELS

The analysis of EIS data is commonly carried out with the aid of equivalent electrical circuit models. The purpose is to determine individual components of the equivalent circuit model that represents the corroding system including metal/solution interface. Figure 5 shows the equivalent circuit models used in this work. For simple corrosion processes, which are under charge transfer control can be described by the electrical circuit (a)[11]. Here R_t is the charge transfer resistance which is inversely proportional to the corrosion rate, R_s is the solution resistance, and C_{dl} is the double layer capacitance that characterizes the charge separation between the metal and electrolyte interface. However the double layer capacitor does not behave ideally. The impedance (Z) of a capacitor has the form:

$$Z = A\,(j\omega)^{-\alpha} \qquad (2)$$

When this equation describes an ideal capacitor, the constant A is equal to 1/C and the exponent $\alpha = 1$. For a non - ideal capacitor, the value of α is less than one. The use of α is only a formal description of non-ideal behavior of double layer, its physical meaning is not clear [11]. Also, this non-ideal behavior of capacitor can be described as Constant Phase Element (CPE). Circuit (a) is also called as CPE model.

Circuit (b) models a cell where electrochemical process includes kinetic and diffusion processes. The experimental phase angle approaches 45° at low frequency, which responds to the diffusion process on the electrode. Diffusion impedance is known as the Warburge impedance, W_d. This impedance depends on the frequency of the potential perturbation. The equation for Wargurg impedance [12] is:

$$W_d = \sigma\,(\omega)^{-1/2}\,(1-j) \qquad (3)$$

Where, σ =Warburg coefficient, ohm.$s^{1/2}$;
$\omega = 2\pi f$, rad.s^{-1}.

For the case of the metal surface that is covered by inhibitor film with pores, circuit (b) is modified to circuit (c). The nested circuit is used to indicate that pores within the inhibited film can cause metallic corrosion by the electrolyte that has direct access to the metal surface. When there are pores on this inhibitor film, the active species of electrolyte can pass through the pores to reach the metal surface. Here C_f is the inhibitor film capacitor, which is a non-ideal capacitor. R_{po} is the pore resistance arising by the formation of ionically conducting paths in the film [12].

RESULTS AND DISCUSSION

Rotating Cylinder Electrode System

Figure 6 shows the EIS spectra of a C-1018 coupon in the presence of 10 ppm corrosion inhibitor at various exposure time in CO_2-saturated 100% saltwater. Figures 6(a)(b)(c) are examples of Nyquist plot, Bode impedance plot, Bode phase plot, respectively. The equivalent electrical circuit model shown in Figure 5(a) was used to interpret metal-solution interface in this case. The shape of Nyquist plot shows one semicircle for the whole period. The solution resistance, R_s, is obtained at an intersection of the semicircle with the real impedance axis on the left side, which corresponds to the impedance modulus at the high frequency in Figures 6(b). The charge transfer resistance, R_t is the size of diameter of the semicircle. Figure 6(a) shows that the diameters of semicircles after the addition of inhibitor are larger than that of the blank test. Figure 6(b), the impedance Bode plot shows the same trend in that R_t is related to the plateau at low frequency on the impedance modulus vs. frequency plot. Separated experiments up to ten hours show that the diameters of the semicircles did not change as significantly as shown in Figure 6(a). Results as shown in Figure 6 indicate that charge transfer resistance increases significantly both after inhibitor addition and increasing time and the larger the charge transfer resistance, Rt, the lower the corrosion rate. Results indicate that the inhibition efficiency increases with time in the test.

Figure 7 shows that the EIS spectra of a C-1018 coupon in the presence of 25 ppm inhibitor in CO2 saturated 100 % seawater. Again the Nyquist plot shows one semicircle shape with or without the present of inhibitor. The charge transfer resistance, R_t increases after addition of inhibitor and increases with time. Compared to Figure 6, charge transfer resistance for 25 ppm concentration is larger than that at 10 ppm at the same immersion time, indicating increasing inhibition efficiency with inhibitor concentration.

It is well known that the imidazoline based inhibitor covers metal surface through the blocking effect. Inhibition effectiveness of a corrosion inhibitor (%η) is often estimated by charge transfer resistance according to the following equation [9]:

$$\%\,\eta = \frac{R_t' - R_t}{R_t'} \times 100\% \qquad (4)$$

where R_t' is the charge transfer resistance in presence of corrosion inhibitor, ohm.cm^2;

R_t is the charge transfer resistance without corrosion inhibitor, ohm.cm^2.

Figure 8 and 9 shows the inhibition efficiency and corrosion rate of this inhibitor package at the whole testing period. The corrosion rate can be calculated as following [13].

$$CR = \frac{\beta_a \times \beta_c}{2.303 \cdot (\beta_a + \beta_c)} \frac{K}{R_t} \qquad (5)$$

Where, CR is the corrosion rate, mm/y;
β_a and β_c are the anodic and catholic Tafel constants, respectively, mV/decade;
K is constant (11.47 is used for metal C-1018 in this work).

The inhibition effectiveness for both concentrations increases with increasing time up to 5 hours, then levels off. The inhibition effectiveness of 25 ppm inhibitor concentration is higher than that at 10 ppm, especially at the very beginning of testing. After 5 hours, the inhibition effectiveness for 10 ppm is close to that of 25 ppm. Corrosion rates for this inhibitor formulation at 25 ppm concentration, as shown in Figure 9, decreases faster than 10 ppm. After five hours, corrosion rates for both concentrations level off to the same value. Table 1 lists some simulation results of the above mentioned tests and corrosion rates at 3.5 hours immersion time.

Multiphase Flow Loop System

With Pre-Corrosion Procedure

Figure 10 shows the comparison of EIS plots in the presence of 25 ppm corrosion inhibitor at various exposure time in CO_2-saturated 100% seawater under slug flow at Froude 9 with the pre-corrosion procedure. Compared to the blank test which shows a simple charge transfer process, the shape of Nyquist curve in Figure 10(a) for inhibitor containing solution at different exposure time shows one semicircle plus a low frequency tail. Circuit 5(b) was used to fit the experimental data and results at 3.5 hours immersion time are listed in Table 2. It can be seen in Table 2 that the change transfer resistance in the flow loop system is much less than in the RCE system for both blank and inhibition tests. The results indicate that the corrosion rates in the flow loop are much greater than that obtained in RCE system. This is resulted from the higher shear stress and turbulence in flowing systems, specially, in the slug flow. Corrosion rates in slug flow are much higher than that in RCE system. The inhibition performance of the inhibitor is reduced in the multiphase flow system.

Figure 10(b) shows that the charge transfer resistance increases with time after the addition of inhibitor, namely the corrosion rate decreases with time. In Figure 10(c), the phase angle at low frequency area approaches slightly to the more negative value with exposure time increasing, which indicates the diffusion process occurring.

Figure 11 shows the comparison of EIS spectra of this model inhibitor at 25 ppm concentration under Froude 9 slug flow with/without pre-corrosion at different exposure times. In Figure 11(a) the shapes of EIS plots without pre-corrosion seem to have another semicircle at high frequency, which might represent the formation of the inhibitor film. The charge transfer resistance increases with immersion time increasing for both cases.

Figure 11(c) shows that the phase angle plots look very different for these two procedures. Another electrochemical process, which might represent film formation, is occurring at high for the case without pre-corrosion. The diffusion process is also found at the low frequency like the case with pre-corrosion. The experimental data without pre-corrosion can be modeled using circuit 5(c). The fitting results are listed in Table 2. The film resistance can be determined for the case without pre-corrosion.

The charge transfer resistance without pre-corrosion is greater than that with pre-corrosion. This means that inhibitor is less effective in the pre-corroded system. This could be explained by the surface roughness as a result of pre-corrosion process. The rough surface hinders inhibitor adsorption on the metal surface, thus reduce inhibitor efficiency. Results show that inhibitor film was not adsorbed well on the rough surface to give good protection and inhibitor give a much better inhibited film on the fresh and smooth surface.

Effects of Flow Patterns for The Case without Pre-corrosion

Figure 12 shows the comparison of experimental results for the model inhibitor at 25 ppm concentration under slug flow at Froude number 6 and 9 and full pipe flow at 0.5 hrs after coupon immersion. The shapes of Nyquist plot for all the cases are typical as observed for the case without pre-corrosion, which can be simulated using circuit 5(c). The Nyquist plot shows that the charge transfer resistance is the smallest for slug flow at Froude number 9 while the charge transfer resistance for full pipe flow and slug flow at Froude number 6 are very similar. This can be expected because the slug flow at lower Froude number 6 has lower turbulence and bubbles cannot reach the pipe wall as observed at Froude number 9. Results suggest that the full pipe flow at 1.25 m/s gives the similar flow effect to that of slug flow at Froude number 6. Some fitting results are also shown in Table 2.

EIS spectra were obtained for the model inhibitor at concentration of 25 ppm for all flow patterns at different immersion time. The amount of data is too great to be presented as EIS plots. Figure 13 and 14 are comparison of charge transfer resistance and diffusion impedance for 25 ppm inhibitor at different flow patterns. The charge transfer resistance for full pipe flow and slug flow at Froude number 6 are very close as observed in Figure 12, with the diameters of semicircle of Nyquist plot being almost the same and the charge transfer resistance being slightly lower for slug flow at Froude number 9. Also as shown in Figure 13, the slug flow at Froude number 9 with pre-corrosion has the lowest charge transfer resistance, which means that corrosion rate is the highest. Again, the results show that inhibitor for a better film on a smoother surface as discussed above. The results obtained for diffusion impedance as shown in Figure 14 seem to give the same tendency as the charge transfer resistance.

CONCLUSIONS

An imidazoline based inhibitor has been tested in a RCE system and pipeline using EIS. The one time constant equivalent electrical circuit was used to simulate the EIS spectra for this model inhibitor in the RCE system. This might suggest that the inhibitor film is uniform under this low shear stress system. Inhibition effectiveness increases with time for the first several hours and then levels off.

The inhibition performance of this model inhibitor was studied in a multiphase pipeline. EIS was used to monitor the corrosion process with/without the inhibitor in multiphase flow. For the cases with pre-corrosion procedure, the circuit with the double layer R_t-C_{dl} network and diffusion impedance, W_d, was used to interpret the electrochemical processes. This means that the corrosion processes under inhibitor effects with pre-corrosion include charge transfer process and diffusion process. EIS spectra did not show the formation of inhibitor films. Compared to results in RCE system, inhibition performance of this inhibitor decrease and corrosion rates in the presence of inhibitor in slug flow increase due to higher shear stress and turbulence.

Circuit (c), which includes film R_{po}-C_f network, double layer R_t -C_{dl} network and diffusion impedance, W_d, describes the corrosion processes without pre-corrosion. Inhibitor film can be detected

on the metal surface for the case without pre-corrosion. The inhibitor performance for protecting corrosion under multiphase flow can be described by an inhibitor film with pores covering the metal surface. The pores within inhibitor film may be resulted from mechanical damage by the turbulence and bubbles impact in multiphase flow. Corrosion rates in slug flow at higher Froude number is larger than slug flow at lower Froude number and full pipe flow. Corrosion rate under inhibition effects is increased in slug flow due to the higher bubble impact and turbulence in multiphase flow.

REFERENCES

1 Choi, H.J., Cepulis R. L., " Inhibitor Film Persistence Measurement by Electrochemical Techniques", SPE Production Engineering, (November), 1987, pp. 325-329.

2 Jepson, W. P., M. Gopal, "The Effect of Pressure, Temperature and Flow Characteristics on Sweet Corrosion in Three Phase Oil/Water/Gas Horizontal Pipelines", Multiphase 95, 7th International Conference, Wilson, A., MEP, London, 1995, pp. 51-76.

3 Sun , Jyi-Yu, Jepson, W. P., "Slug Flow Characteristics and Their Effect on Corrosion Rates in Horizontal Oil and Gas Pipelines", SPE Paper 24787, 1992, pp.215-228.

4 Green, A. S., Johnson, B. V., and Choi, H.J., " Flow Relation Corrosion in Large Diameter Multiphase Flow Pipeline", SPE Paper 20685, 1989, pp. 677-684.

5 Zhou, X., Jepson, W. P., "Corrosion in Three Phase Oil/Water/Gas Slug Flow in Horizontal Pipes", NACE CORROSION/94, Paper No. 94026, 1994.

6 Gopal, M., Kaul, A., Jepson, W. P., " Mechanism Contributing to Enhanced Corrosion in Three Phase Slug Flow in Horizontal Pipes", NACE CORROSION/95, Paper No.105, 1995.

7 Chen, Y., Jepson, W. P., "Comparison of ECN and EIS Measurement for Corrosion Monitoring under Multiphase Flow Condition", NACE CORROSION/97, Paper No.347, 1997.

8 Chen, H, "A Evaluation of Oil Field Corrosion Inhibitors by EIS", NACECORROSION/94, Paper No.32, 1994.

9 Cao, C., "On Electrochemical Techniques For Interface Inhibitor Research", Corrosion Science, **38**, No.12, 1996, pp. 2073.

10 Jepson, W. P., " Flow Characteristics in Horizontal Slugs", 3rd Int. Conf. On Multiphase Flow, The Hague, Netherlands, 1987, pp. 187-197.

11 Mansfeld, F., Shih, H. et al., " Analysis of EIS Data Common Corrosion Processes" , Electrochemical Impedance: Analysis and Interpretation, ASTM STP 1188, Scully, J. R., et al., Philadelphia,1993, pp. 37-53.

12 Walter, G. W., " A review of Impedance Plot Methods Used for Corrosion Performance Analysis of Painted Metals ", Corrosion Science , **26,** No. 9, 1986, pp. 681-703.

13 Tait, W. S., An Introduction to Electrochemical Corrosion Testing for Practicing Engineers and Scientists , Pair ODocs Publications, 1994, pp48-49.

TABLE 1 – Comparison of fitting results for RCE and Froude number 9 slug flow with pre-corrosion at 3.5 hours immersion time

System	[CI] ppm	Model	Simulation results			%η	Tafel constants		CR mm/yr
			Rs ohm. cm^2	Rt ohm. cm^2	W_d ohm $s^{1/2}$		β_a mV/decd	β_c mV/decd	
RCE	0	a	2.0	97.4	--	--	72.1	240.4	2.63
RCE	10	a	4.2	309.6	--	68.5	98.4	194.3	1.05
RCE	25	a	17.2	811.8	--	88.0	106.2	160.2	0.39
Flow loop Fr=9 slug	0	a	4.8	47.4	--	--	46.8	205.1	4.0
Flow loop Fr=9 slug	25	b	4.9	182.7	27.9	74.1	93.1	101.1	1.32

Notes, (1) The blank tests for RCE and pipeline are the separated experiment

(2) $\%\eta = \frac{R_t' - R_t}{R_t'} 100\%$, R_t' is the charge transfer resistance in presence of corrosion inhibitor and R_t is the charge transfer resistance without corrosion inhibitor for the separated blank tests

(3) The Tafel curve measurements were taken following EIS tests at 3.5 hour of immersion time for all set of experiments.

TABLE 2 - Comparison of fitting results for flow loop at different flow patterns at 3.5 hour immersion time

Flow pattern	[Cl] ppm	Model	Simulation results			%η	Tafel constants		CR mm/yr
			R_s ohm. cm^2	R_t ohm. cm^2	W_d ohm. cm^2		β_a mV/decd	β_c mV/decd	
Fr=9 slug	0	a	4.7	47.4	--	--	46.8	205.1	4.00
Fr=6 slug	0	a	4.7	51.7	--	--	41.8	277.9	3.50
Full pipe	0	a	4.7	73.7	--	--	45.5	300.4	2.67
Fr=9 slug*	25	b	4.9	182.7	27.9	74.1	93.1	101.1	1.32
Fr=9 slug	25	c	4.1	252	37.7	81.2	120.4	118.2	1.18
Fr=6 slug	25	c	3.0	285	32.1	81.9	130.9	115.4	1.07
Full pipe	25	c	5.2	288	38.5	74.4	124.7	112.3	1.02

Notes, (1) The blank tests for RCE and pipeline are the separated experiments

(2) $\%\eta = \frac{R_t' - R_t}{R_t'} 100\%$, R_t' is the charge transfer resistance in presence of corrosion inhibitor and R_t is the charge transfer resistance without corrosion inhibitor for the separated blank tests

(3) Tafel curve measurements were taken following EIS tests at 3.5 hour of immersion time for all set of experiments.

(4) * indicates the test with pre-corrosion procedure

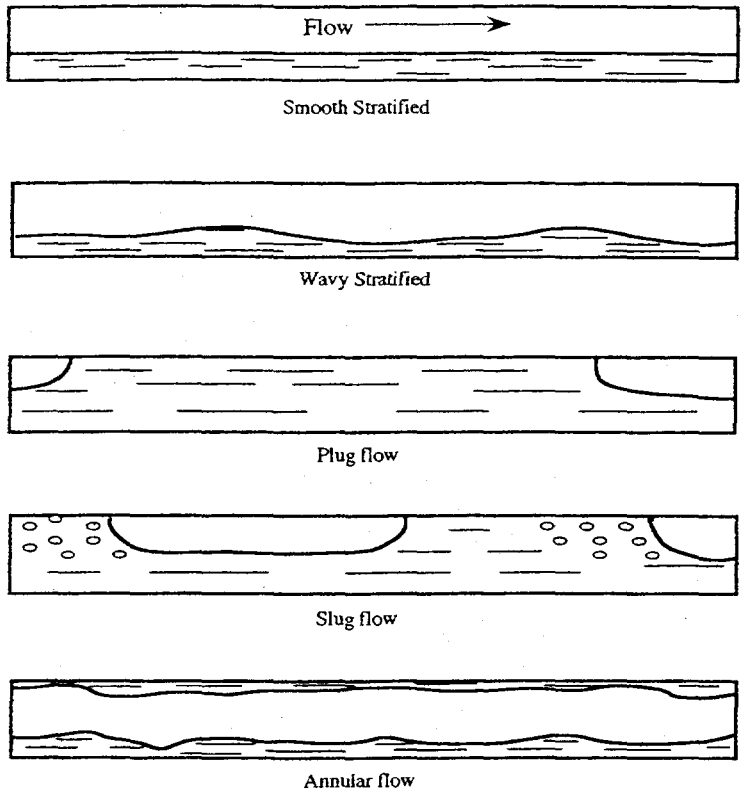

FIGURE 1 - Flow patterns in water/gas horizontal pipes

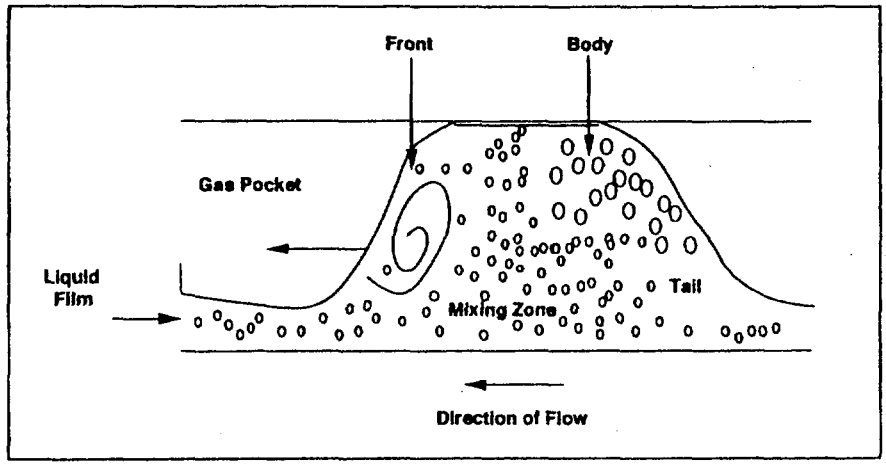

FIGURE 2 - Profile of a slug

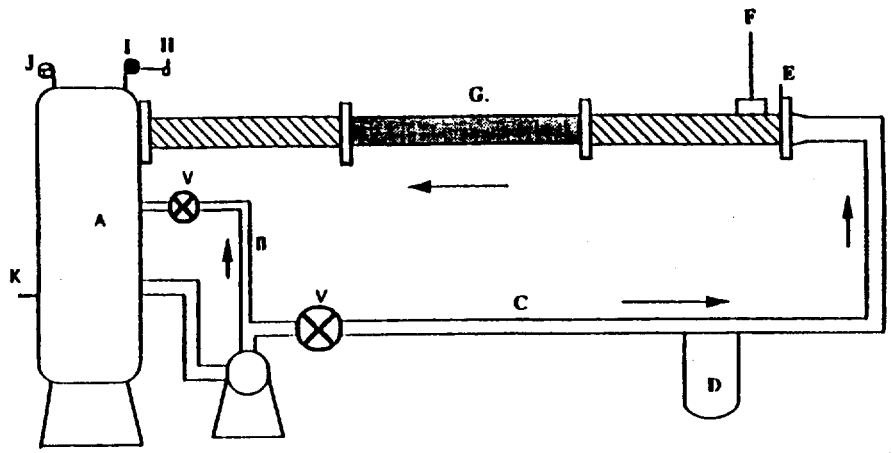

A. Liquid tank
B. Liquid recycle
C. Liquid feed
D. Orifice plate with pressure pipe
E. Flow height control gate
F. Carbon dioxide feed line
G. Test section
H. Gas outlet with filters
I. Pressure gauge with back pressure control
K. Heater
V. Flow control valve

FIGURE 3a – Experimental pipeline system

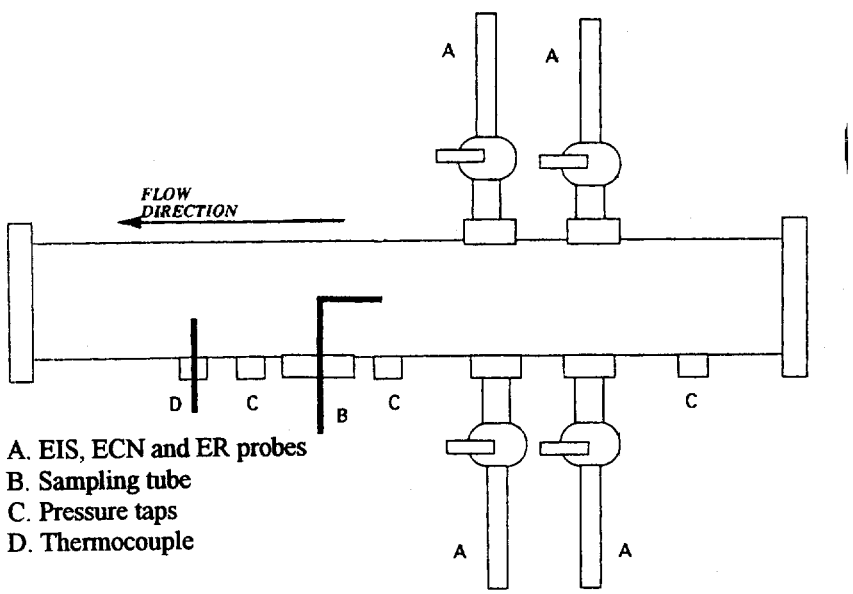

A. EIS, ECN and ER probes
B. Sampling tube
C. Pressure taps
D. Thermocouple

FIGURE 3b – Test section

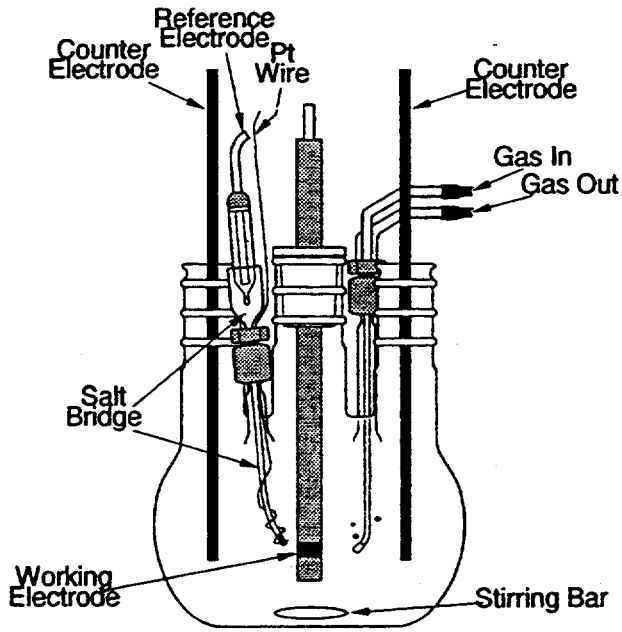

FIGURE 4a – Rotating Cylinder Electrode cell

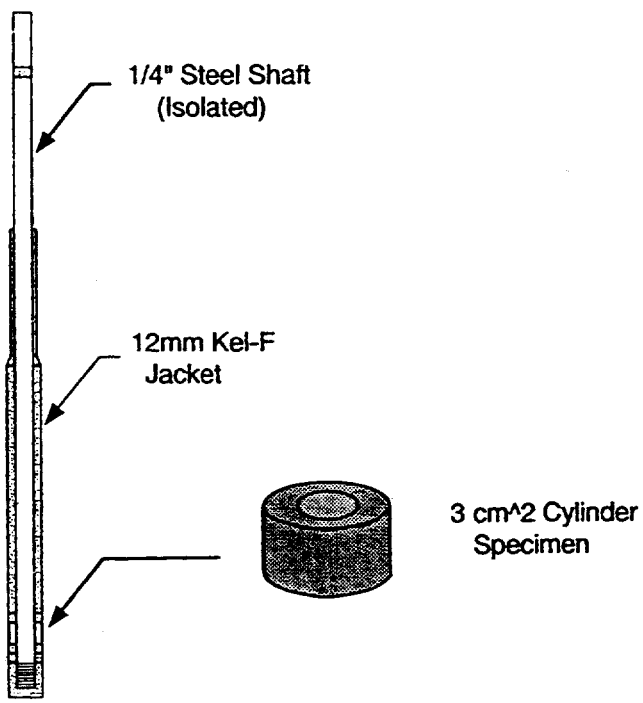

FIGURE 4b – Electrode assembly used in RCE system

(a)

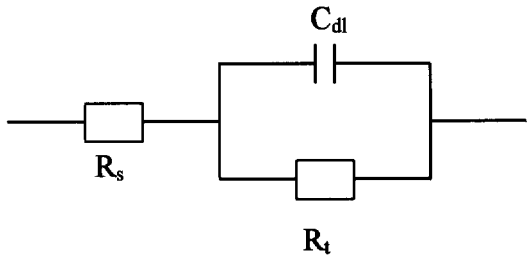

(b)

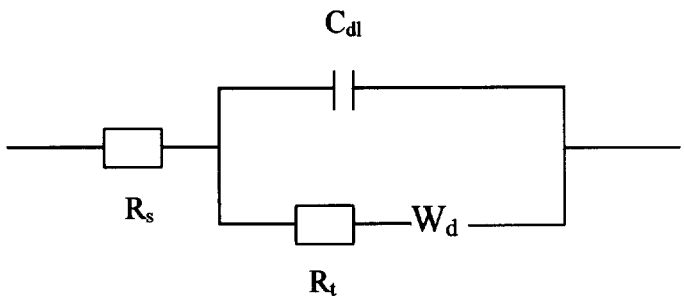

(c)

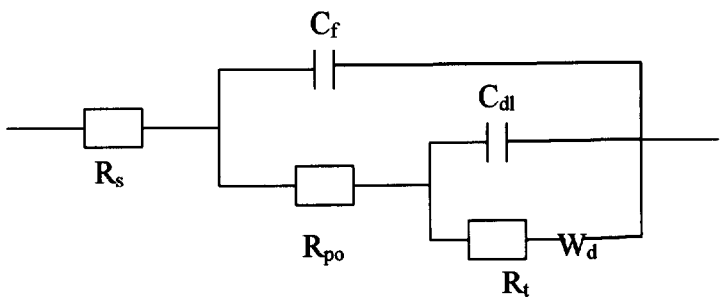

FIGURE 5 - Equivalent circuit models used in this work

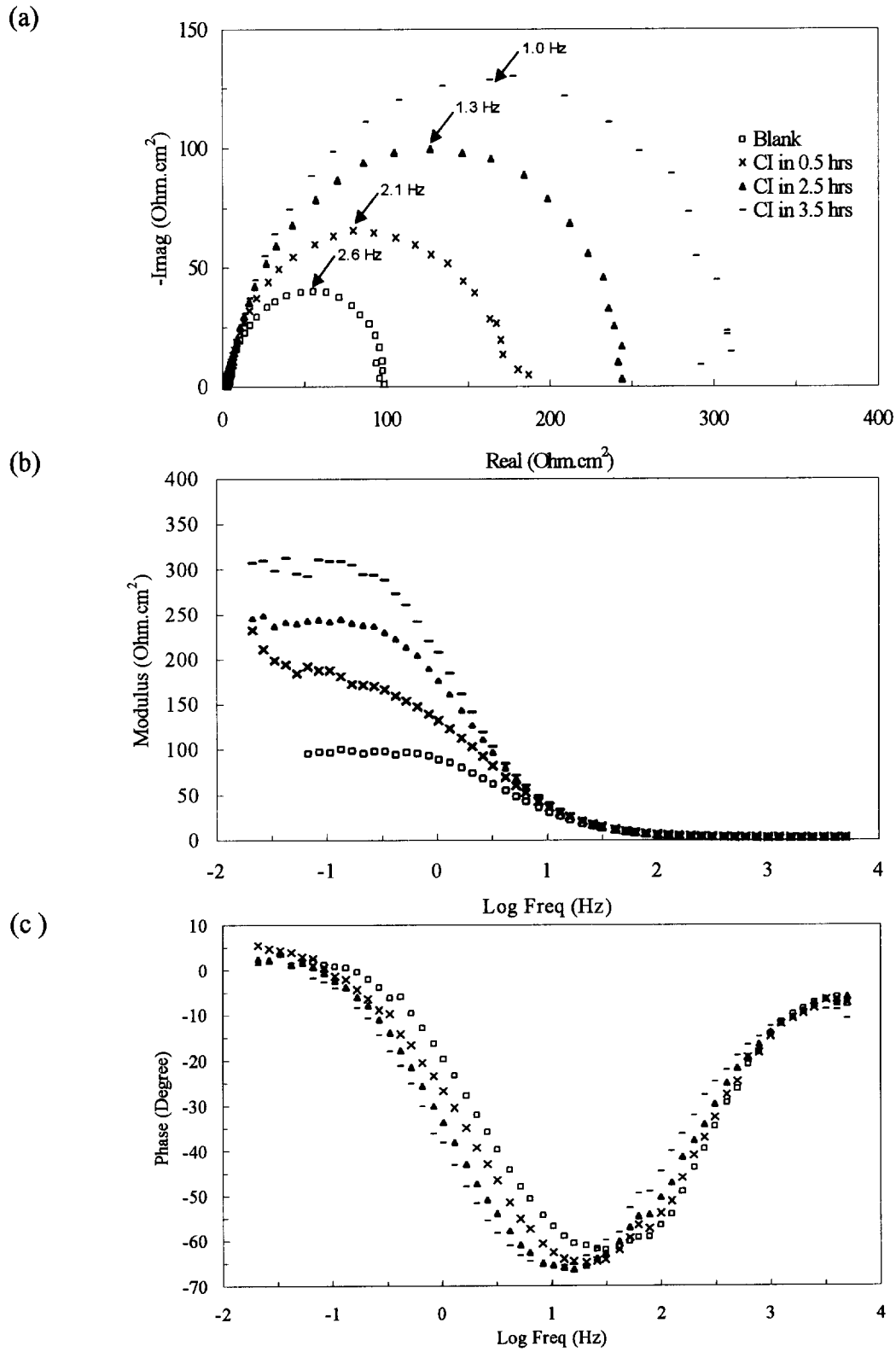

FIGURE 6 - EIS spectra for C-1018 at 10ppm inhibitor in 100% saltwater RCE system (a) Nyquist plot (b) Bode impedance plot (c) Bode phase plot

(a)

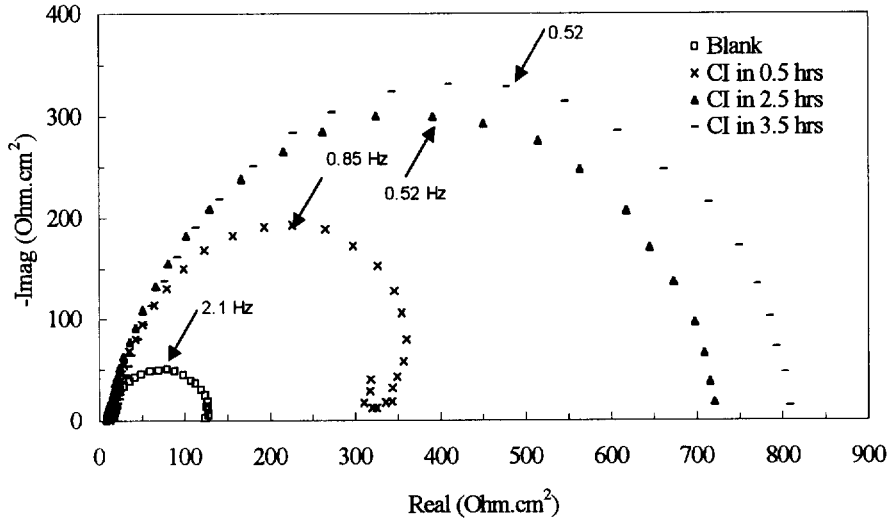

(b)

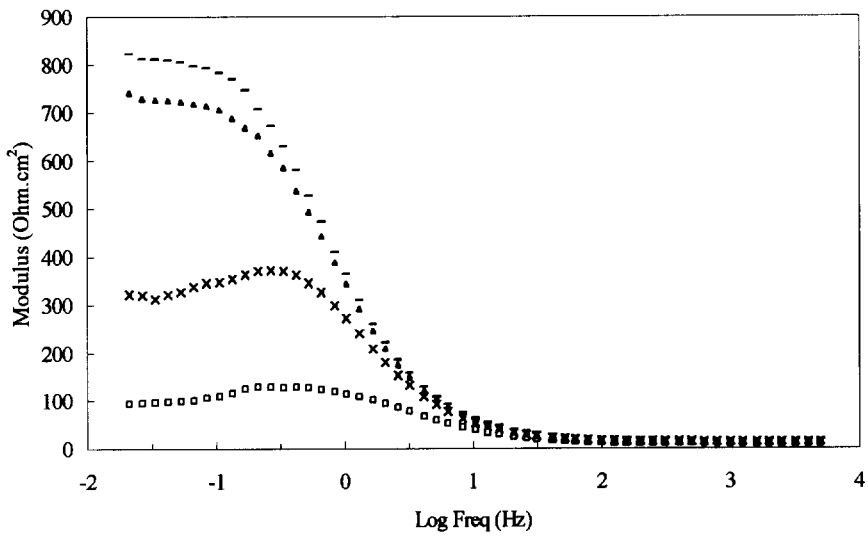

(c)

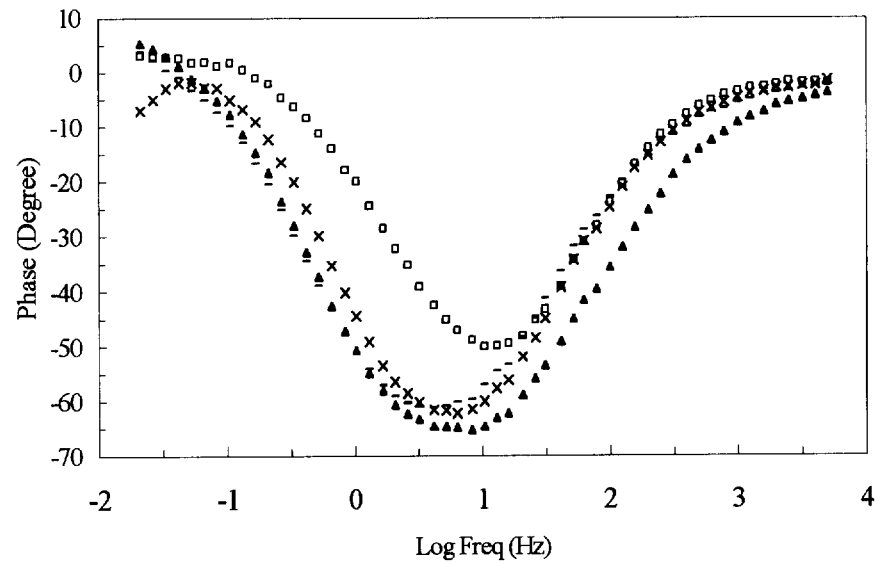

FIGURE 7 - EIS spectra for C-1018 at 25ppm inhibitor in 100% saltwater RCE system (a) Nyquist plot (b) Bode impedance plot (c) Bode phase plot

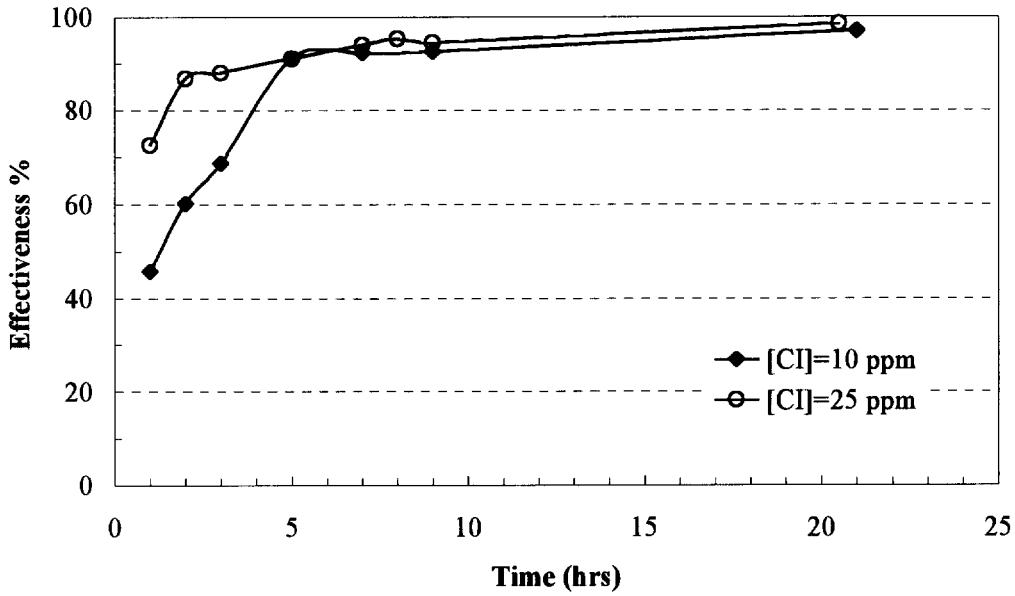

FIGURE 8 – Inhibition effectiveness for model inhibitor in the RCE system

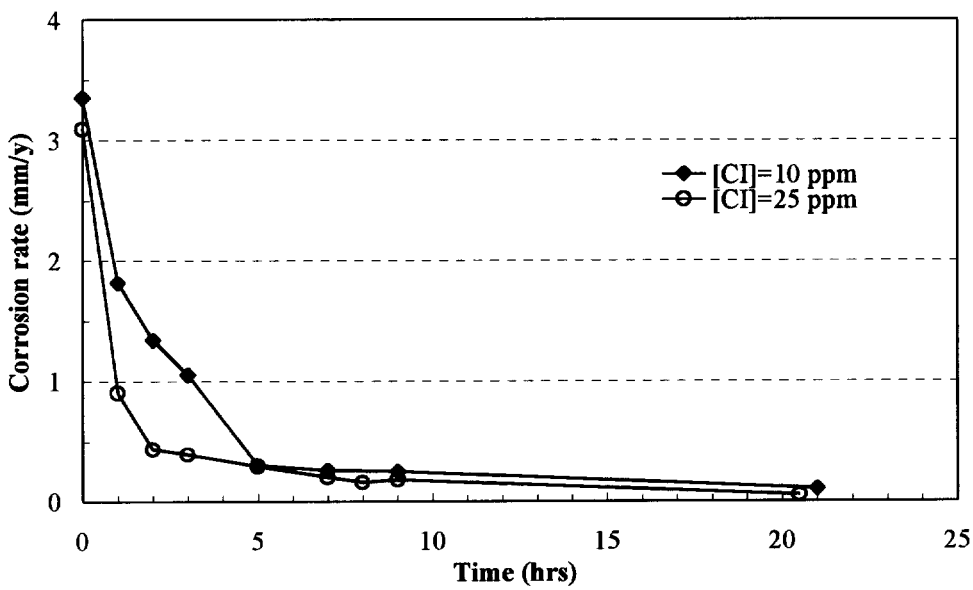

FIGURE 9 Corrosion rate for model inhibitor in the RCE system

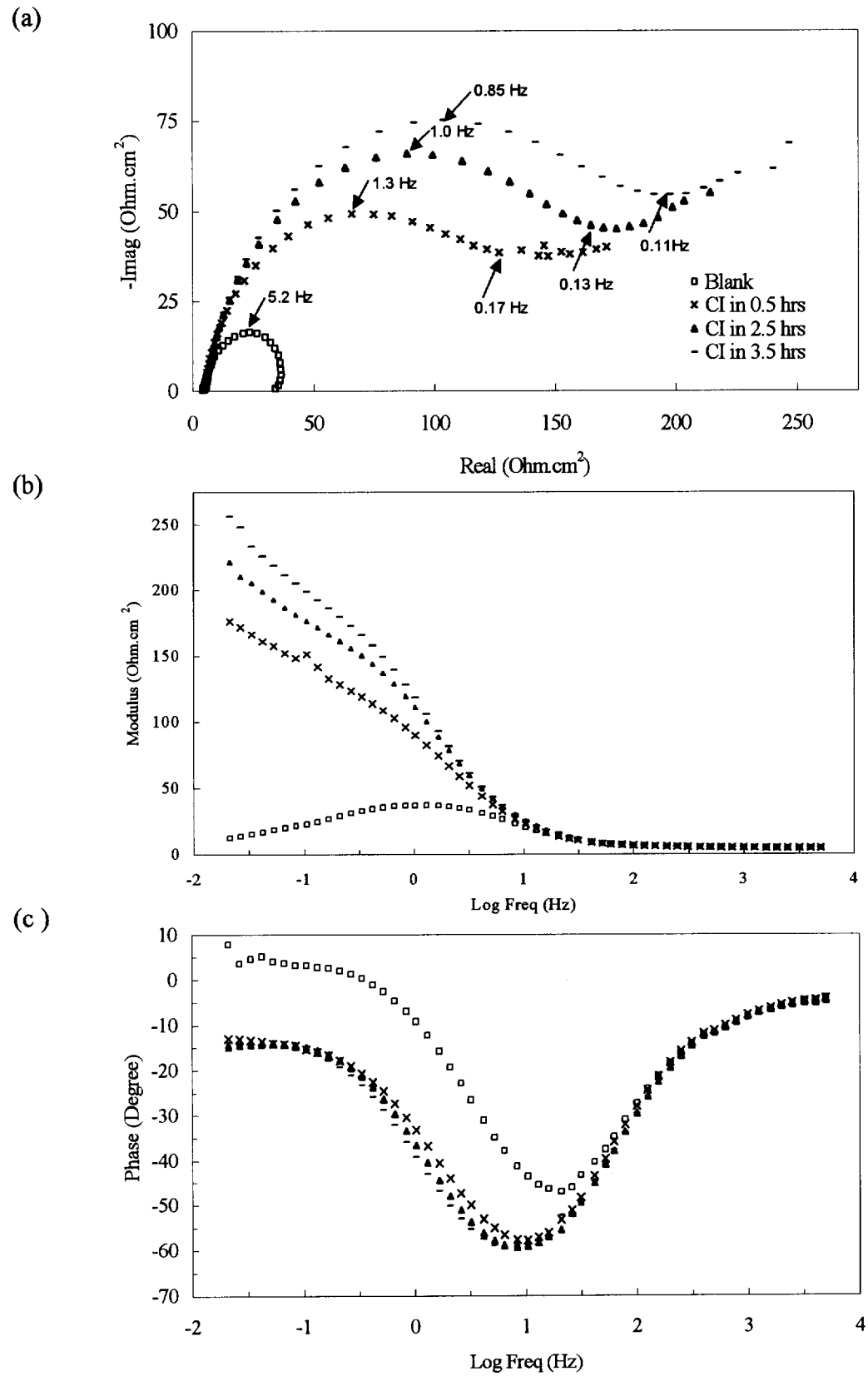

FIGURE 10 - EIS spectra for C-1018 at 25ppm inhibitor in 100% saltwater Froude 9 slug flow system (a) Nyquist plot (b) Bode impedance plot (c) Bode phase plot

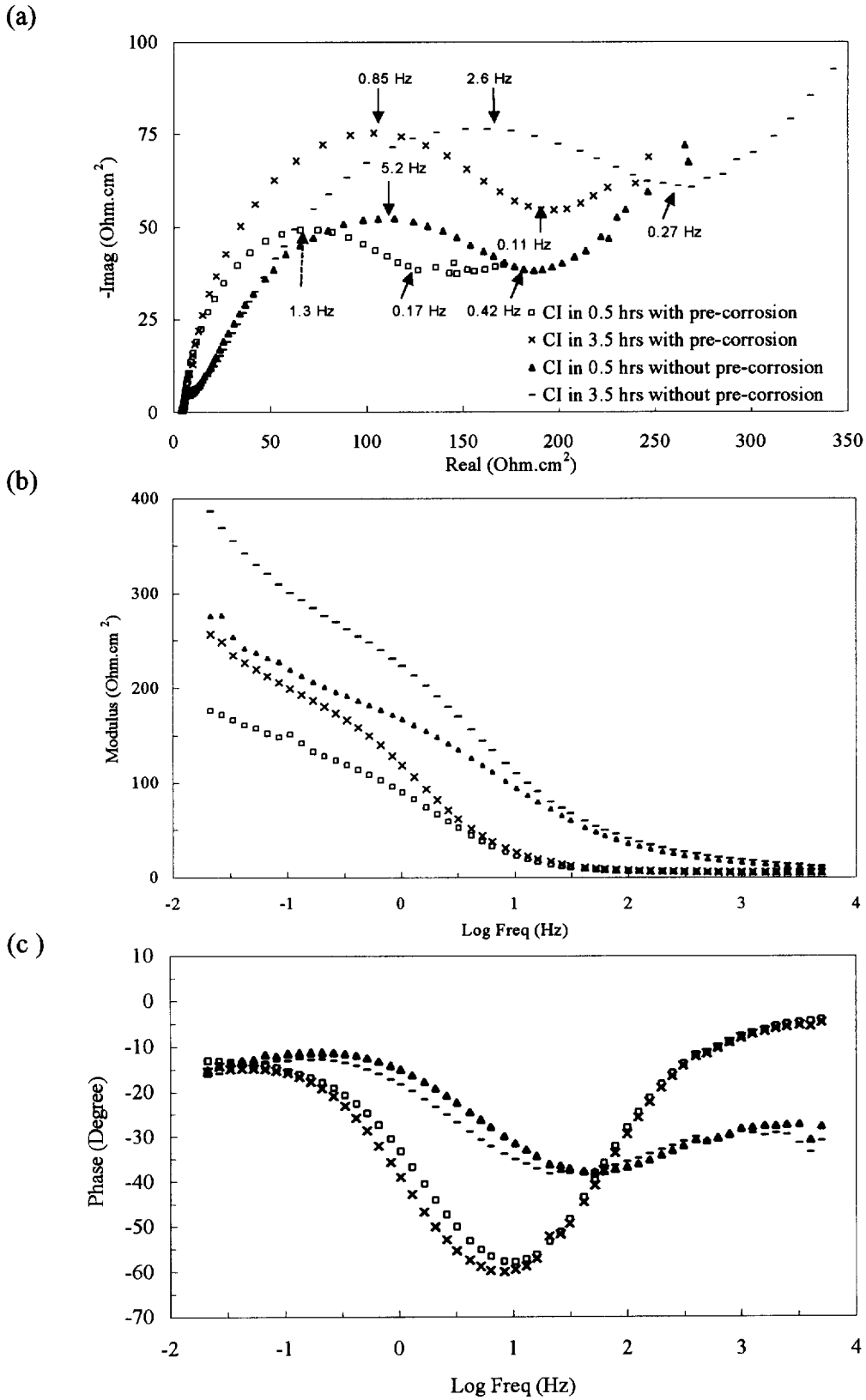

FIGURE 11- Comparison of EIS spectra for C-1018 at 25ppm inhibitor in 100% saltwater Froude 9 slug flow system (a) Nyquist plot (b) Bode impedance plot (c) Bode phase plot

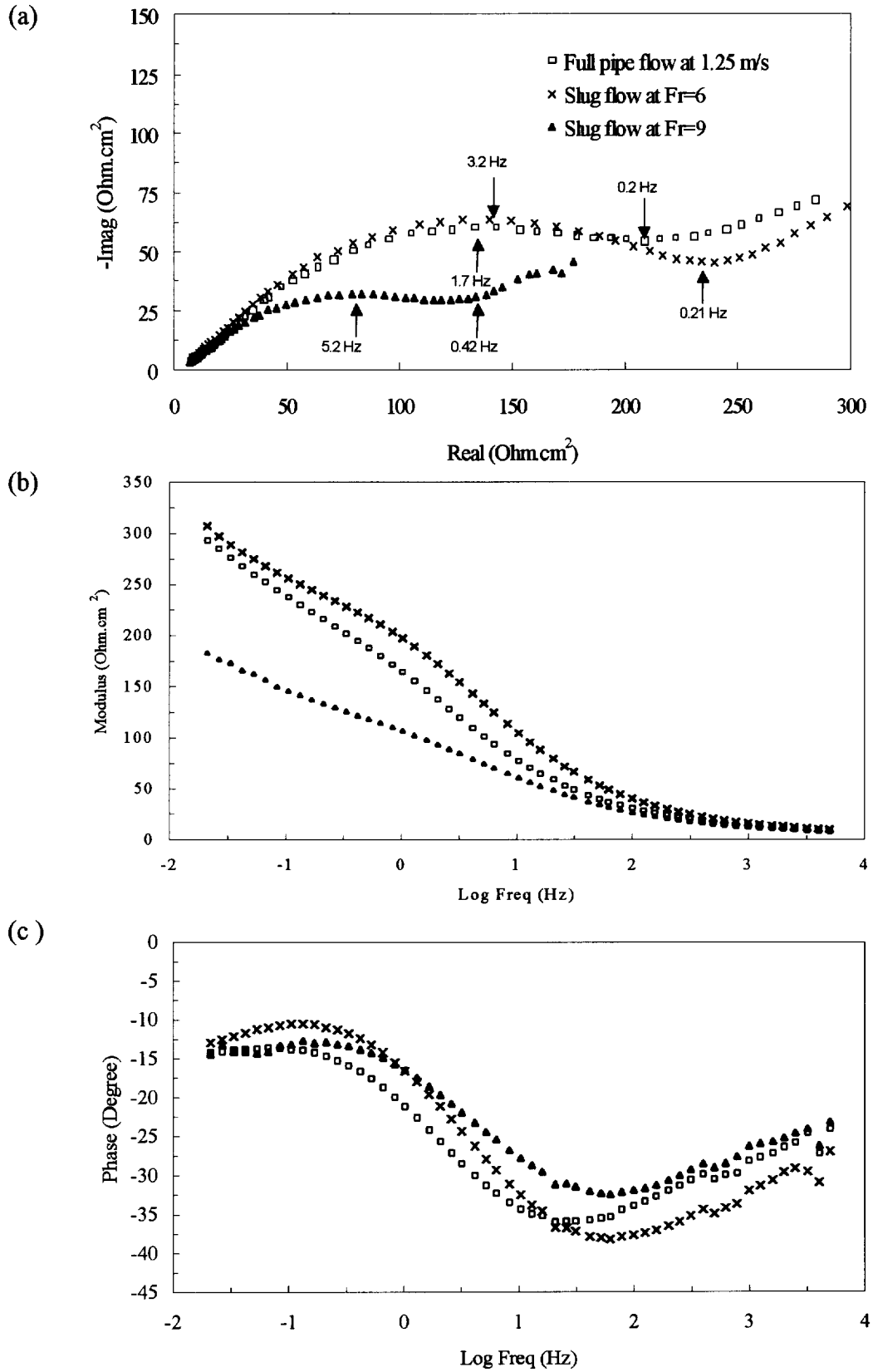

FIGURE 12 - Comparison of EIS spectra for C-1018 at 25ppm inhibitor in 100% saltwater pipeline at different flow patterns(a) Nyquist plot (b) Bode impedance plot (c) Bode phase plot

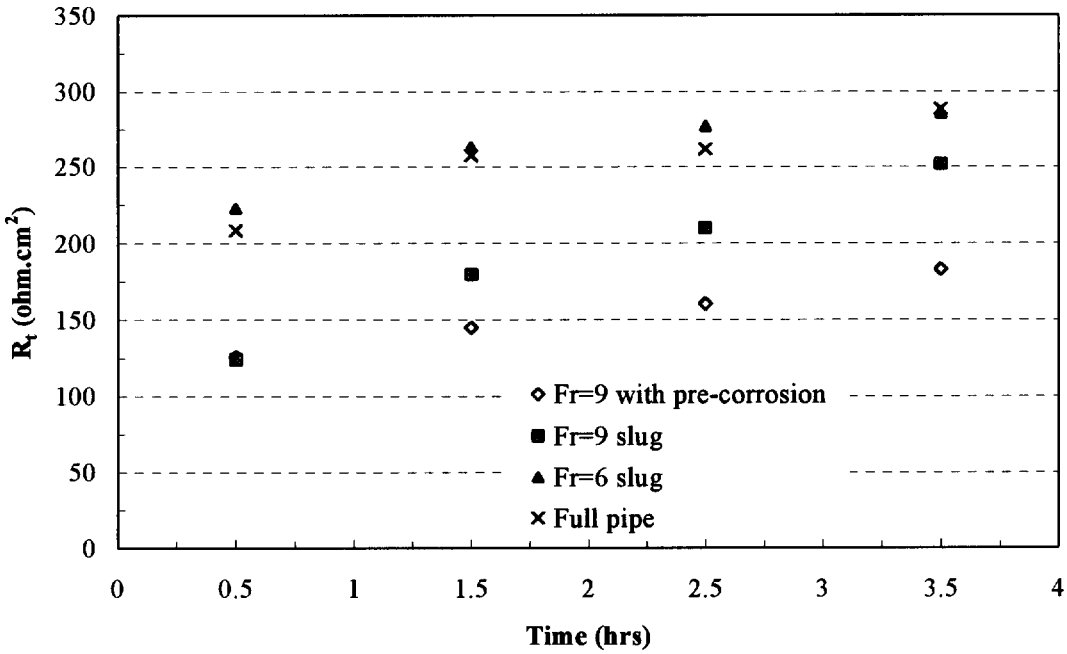

FIGURE 13 – Comparison of R_t in the pipeline at different experimental conditions

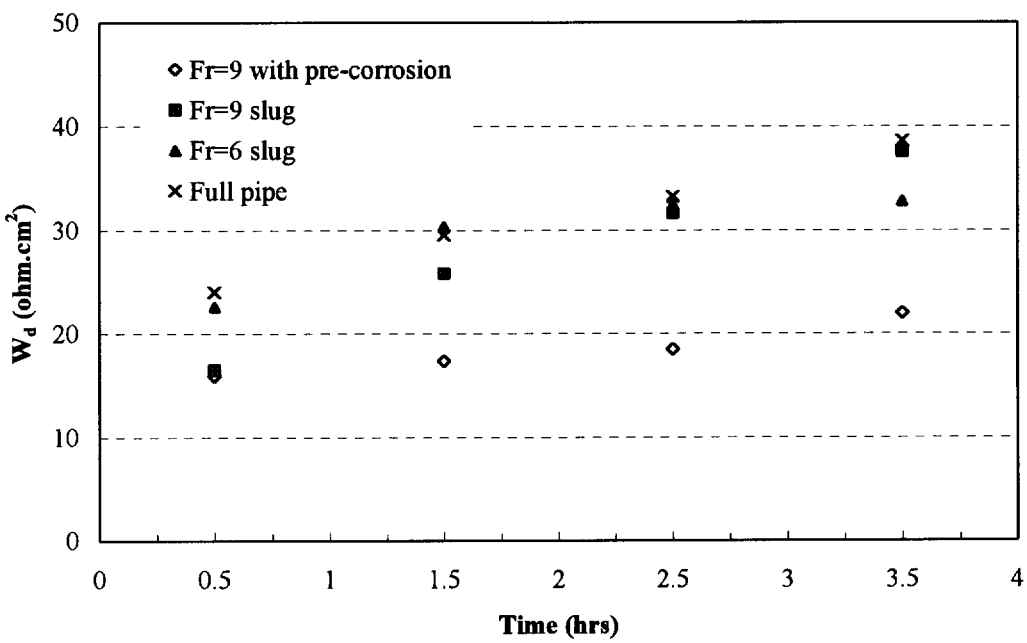

FIGURE 14 – Comparison of W_d in the pipeline at different experimental conditions